Inorganic Chemistry

Article

pubs.acs.org/IC

Fluoride-Ion Acceptor Properties of WSF_4: Synthesis, Characterization, and Computational Study of the WSF_5^- and $W_2S_2F_9^-$ Anions and ^{19}F NMR Spectroscopic Characterization of the $W_2OSF_9^-$ Anion

Jared Nieboer,[†] Ralf Haiges,[‡] William Hillary,[†] Xin Yu,[†] Tyler Richardet,[†] Hélène P. A. Mercier,[§] and Michael Gerken*,[†]

[†]Department of Chemistry and Biochemistry, The University of Lethbridge, Lethbridge, Alberta T1K 3M4, Canada

[‡]Loker Hydrocarbon Institute, University of Southern California, Los Angeles, California 90089, United States

[§]Department of Chemistry, McMaster University, Hamilton, Ontario L8S 4M1, Canada

Supporting Information

ABSTRACT: The new $[N(CH_3)_4][WSF_5]$ salt was synthesized by two preparative methods: (a) by reaction of WSF_4 with $[N(CH_3)_4][F]$ in CH_3CN and (b) directly from WF_6 using the new sulfide-transfer reagent $[N(CH_3)_4][SSi(CH_3)_3]$. The $[N(CH_3)_4][WSF_5]$ salt was characterized by Raman, IR, and ^{19}F NMR spectroscopy and $[N(CH_3)_4][WSF_5]\cdot CH_3CN$ by X-ray crystallography. The reaction of WSF_4 with half an aliquot of $[N(CH_3)_4][F]$ yielded $[N(CH_3)_4][W_2S_2F_9]$, which was characterized by Raman and ^{19}F NMR spectroscopy and by X-ray crystallography. The WSF_5^- and $W_2S_2F_9^-$ anions were studied by density functional theory calculations. The novel $[W_2OSF_9]^-$ anion was observed by ^{19}F NMR spectroscopy in a CH_3CN solution of WOF_4 and WSF_5^-, as well as CH_3CN solutions of WSF_4 and WOF_5^-.

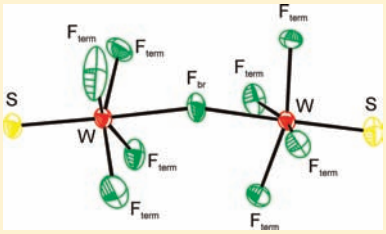

INTRODUCTION

Tungsten sulfide tetrafluoride, WSF_4, has been known to act as a Lewis acid, as documented by formation of the $WSF_4\cdot CH_3CN$ and $WSF_4\cdot NC_5H_5$ adducts and the fluorine bridging observed in solid WSF_4.[1,2] While the fluoride-ion acceptor properties of WSF_4 have not been studied, the anions WSF_5^- and $W_2S_2F_9^-$ have been observed in acetonitrile solutions by ^{19}F NMR spectroscopy in an admixture with other anionic and neutral tungsten species.[3,4] The synthetic routes to the WSF_5^- and $W_2S_2F_9^-$ anions have utilized fluoride−chloride substitution, starting from $WSCl_4$ and HF or F^-.[3−5] An X-ray crystal structure of $[\{(C_6H_5)_3P\}_2N][WSF_5]\cdot CH_3CN$ showed a pseudooctahedral WSF_5^- anion, which was prepared from $WSCl_4$ and NaF.[5] In the present study, the fluoride-ion acceptor properties of WSF_4 are investigated systematically.

RESULTS AND DISCUSSION

Synthesis of $[N(CH_3)_4][WSF_5]$. The new $[N(CH_3)_4][WSF_5]$ salt was prepared by the addition of $[N(CH_3)_4][F]$ to WSF_4 in CH_3CN at −40 °C according to eq 1. Upon removal of the solvent under dynamic vacuum, a beige solid was obtained. The solid, $[N(CH_3)_4][WSF_5]$, is stable at ambient temperature under exclusion of moisture and was characterized by Raman and ^{19}F NMR spectroscopy. The WSF_5^- anion was found to be moderately soluble in CH_3CN, producing a bright-yellow solution.

$$WSF_4 + [N(CH_3)_4][F] \xrightarrow{CH_3CN} [N(CH_3)_4][WSF_5] \quad (1)$$

Alternatively, the new sulfide-transfer agent, $[N(CH_3)_4][SSi(CH_3)_3]$, can be utilized for the synthesis of $[N(CH_3)_4][WSF_5]$. The $N(CH_3)_4^+$ salt of the trimethylsilylthiolate anion was prepared from $S(Si(CH_3)_3)_2$ and $[N(CH_3)_4][F]$ in CH_3CN according to eq 2.

$$S(Si(CH_3)_3)_2 + [N(CH_3)_4][F] \xrightarrow{CH_3CN} [N(CH_3)_4][SSi(CH_3)_3] + FSi(CH_3)_3 \quad (2)$$

The $[N(CH_3)_4][SSi(CH_3)_3]$ salt is a white moisture-sensitive solid that is extremely malodorous when exposed to the atmosphere. It is sparingly soluble in CH_3CN and tetrahydrofuran (THF). Reacting $[N(CH_3)_4][SSi(CH_3)_3]$ directly with WF_6 in THF at −78 °C yielded $[N(CH_3)_4][WSF_5]$ according to eq 3.

$$[N(CH_3)_4][SSi(CH_3)_3] + WF_6 \xrightarrow{THF} [N(CH_3)_4][WSF_5] + FSi(CH_3)_3 \quad (3)$$

To our knowledge, only the sodium salt of trimethylsilylthiolate has been reported.[6,7] The $Na[SSi(CH_3)_3]$ salt has been used as a reagent in inorganic oxide/sulfide substitution reactions and in a number of organic reactions.[6,7]

Synthesis of $[N(CH_3)_4][W_2S_2F_9]$ and Formation of the $W_2OSF_9^-$ Anion. The reaction of WSF_4 with $[N(CH_3)_4][F]$ in

Received: March 20, 2012
Published: May 16, 2012

   dx.doi.org/10.1021/ic3005882 | Inorg. Chem. 2012, 51, 6350−6359

a 2:1 ratio in CH_3CN yielded brown $[N(CH_3)_4][W_2S_2F_9]$ containing the fluorine-bridged dinuclear $W_2S_2F_9^-$ anion (eq 4), which was identified by Fluorine-19 NMR and Raman spectroscopy. ^{19}F NMR spectroscopy (vide infra) of a CH_3CN solution showed the presence of WSF_5^- and $WSF_4{\cdot}CH_3CN$ besides $W_2S_2F_9^-$, indicating that equilibrium (5) is operative in CH_3CN solvent. In anhydrous HF, the WSF_5^- anion reacts with the solvent to give the $W_2S_2F_9^-$ anion (eq 6).

$$2WSF_4 + [N(CH_3)_4][F] \xrightarrow{CH_3CN} [N(CH_3)_4][W_2S_2F_9] \quad (4)$$

$$[N(CH_3)_4][W_2S_2F_9] + CH_3CN \overset{CH_3CN}{\rightleftharpoons} WSF_4{\cdot}CH_3CN + [N(CH_3)_4][WSF_5] \quad (5)$$

$$2WSF_5^- + HF \rightarrow W_2S_2F_9^- + HF_2^- \quad (6)$$

The presence of small amounts of water in a sample of $[N(CH_3)_4][W_2S_2F_9]$ in CH_3CN solvent resulted in hydrolysis and formation of WOF_5^-, traces of $W_2O_2F_9^-$, as well as the novel $W_2OSF_9^-$ anion. Attempts to prepare CH_3CN solutions containing mainly the $W_2OSF_9^-$ anion utilized reactions of equimolar amounts of WSF_4 and $[N(CH_3)_4][WOF_5]$ (eq 7), as well as of WOF_4 and $[N(CH_3)_4][WSF_5]$ (eq 8) in CH_3CN solvent. The resulting solutions, however, contained mixtures of $W_2OSF_9^-$ with the mono- and dinuclear oxide fluoride and sulfide fluoride anions and $WSF_4{\cdot}CH_3CN$, confirming equilibria (5) and (7) and an analogous equilibrium between the oxide fluoride anions in CH_3CN solvent. The absence of the ^{19}F NMR resonance attributable to $WOF_4{\cdot}CH_3CN$ indicates the higher Lewis acidity of WOF_4 toward F^- compared to WSF_4.

$$WSF_4{\cdot}CH_3CN + [N(CH_3)_4][WOF_5] \rightleftarrows [N(CH_3)_4][W_2OSF_9] + CH_3CN \quad (7)$$

$$WOF_4 + [N(CH_3)_4][WSF_5] \rightarrow [N(CH_3)_4][W_2OSF_9] \quad (8)$$

Vibrational Spectroscopy. The salts $[N(CH_3)_4][WSF_5]$, $[N(CH_3)_4][W_2S_2F_9]$, and $[N(CH_3)_4][SSi(CH_3)_3]$ were characterized by IR and Raman spectroscopy. The assignments for the $N(CH_3)_4^+$ cation follow those previously given for other $N(CH_3)_4^+$ salts.[8,9] The IR and Raman spectra of $[N(CH_3)_4][SSi(CH_3)_3]$ are shown in Figure S2 in the Supporting Information, and the vibrational frequencies are listed in Table S2 in the Supporting Information. The most intense band in the Raman spectrum of $[N(CH_3)_4][SSi(CH_3)_3]$ at 509 cm^{-1}, together with its strong IR counterpart at 508 cm^{-1}, corresponds to the Si−S stretching mode. This band appears at substantially higher frequency than the symmetric and asymmetric stretching bands of the $S(Si(CH_3)_3)_2$ precursor (484 and 437 cm^{-1}), reflecting stronger Si−S bonding in the thiolate anion.[10]

a. [N(CH$_3$)$_4$][WSF$_5$]. The vibrational spectra of $[N(CH_3)_4][WSF_5]$ at room temperature are depicted in Figure 1, and the experimental and calculated vibrational frequencies for the WSF_5^- anion are listed in Table 1, together with their assignments. Overall, the calculated vibrational frequencies at the B3LYP and PBE1PBE levels of theory are in good agreement with the experimental values. The assignments of the Raman and IR bands are based on the calculated vibrational frequencies and signal intensities.

The most intense band in the Raman spectrum of $[N(CH_3)_4][WSF_5]$ appears at 520 cm^{-1} and can be attributed to the W═S stretching mode. This frequency is in close agreement with the previously reported W═S stretching frequency for [Na(15-crown-5)][WSF_5] (525 cm^{-1}).[5] It is significantly lower than that for monomeric WSF_4 in HF solvent (563 cm^{-1}) and of solid polymeric WSF_4 (578 cm^{-1}),[1] suggesting a weakened W═S bond in the anion, and even lower than that of the $WSF_4{\cdot}NC_5H_5$ adduct (539 cm^{-1}),[2] reflecting the stronger Lewis basicity of the "naked" fluoride ion compared to pyridine. The medium-intensity Raman band at 664 cm^{-1}, with its IR counterpart at 662 cm^{-1}, can be assigned to the symmetric WF_5 stretching mode. This W−F stretching band is shifted to lower frequency compared to that of monomeric WSF_4 in HF solvent (690 cm^{-1}) and $WSF_4{\cdot}NC_5H_5$ (674 cm^{-1}), agreeing with more ionic W−F bonding in the anion. The very strong IR bands at 598 and 532 cm^{-1} correspond to the W−F stretching modes, $\nu_8(E)$ and $\nu_2(A_1)$, respectively. The vibrational frequencies and the large IR and very small Raman intensities that were calculated for these modes are in excellent agreement with the observation of these modes only by IR spectroscopy. The medium-intensity Raman band observed at 292 cm^{-1} is assigned to the S−W−F bending mode and appears at higher frequency than that for monomeric WSF_4 (241 cm^{-1}). The assignments of the Raman bands at 220 and 131 cm^{-1} to the WF_4 scissoring vibration and the S−W−F_{ax} rocking mode are based on their calculated relative Raman intensities. Significantly higher and lower calculated frequencies for the WF_4 scissoring vibration and the S−W−F_{ax} rocking mode, respectively, have also been observed for monomeric WSF_4.[1]

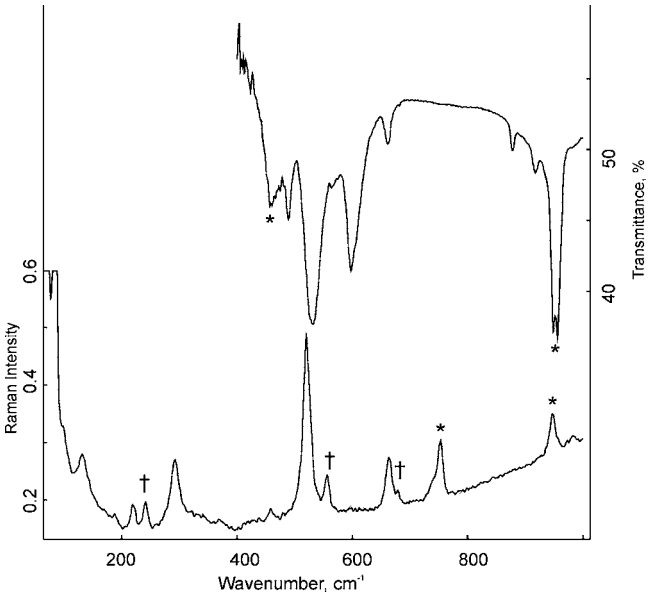

Figure 1. Vibrational spectra of $[N(CH_3)_4][WSF_5]$: IR spectrum (upper trace) recorded at room temperature as a KBr pellet and Raman spectrum (lower trace) recorded at −100 °C using 1064-nm excitation. Asterisks (*) and daggers (†) denote $N(CH_3)_4^+$ cation bands and bands arising from an $W_2S_2F_9^-$ impurity, respectively.

b. [N(CH$_3$)$_4$][W$_2$S$_2$F$_9$]. The IR and Raman spectra of $[N(CH_3)_4][W_2S_2F_9]$ are depicted in Figure 2, and the experimental and calculated vibrational frequencies for the $W_2S_2F_9^-$ anion are given in Table 2, together with their assignments. The calculated vibrational frequencies are in good agreement with the experimental values, and the assignments of the Raman and IR bands are based on the calculated vibrational frequencies and signal intensities.

dx.doi.org/10.1021/ic3005882 | Inorg. Chem. 2012, 51, 6350−6359

Table 1. Observed and Calculated Vibrational Frequencies for WSF_5^- and Their Assignments in the C_{4v} Point Group

frequencies for WSF_5^-, cm^{-1}				
exptl[a,b]			calcd[c]	
Raman[b]	IR[d]	IR[e]	B3LYP	assignment (C_{4v})
664 (28)	662 m	662 s	653 (14) [92]	$\nu_1(A_1)$, $\nu_s(WF_5)$
	598 vs	607 vs, br	608 (<1) [264]	$\nu_8(E)$, $\nu_{as}(WF_{4,eq})$
			572 (4) [0]	$\nu_5(B_1)$, $\nu_{as}(WF_{4,eq})$
527 sh	532 vs	526 s	513 (2) [215]	$\nu_2(A_1)$, $\nu(WF_{5,ax})$
520 (100)			498 (44) [75]	$\nu_3(A_1)$, $\nu(WS)$
	490 m	472 s, br		combination mode
292 (38)			292 (3) [8]	$\nu_9(E)$, $\delta(WF1F4F5) + \delta(WF2F3S)$
			281 (<1) [19]	$\nu_4(A_1)$, $\delta_{umbrella}(WF_{4,eq})$
220 (13)			281 (2) [0]	$\nu_6(B_2)$, $\delta_{scissoring}(WF_{4,eq})$
			217 (<1) [22]	$\nu_{10}(E)$, $\delta(F2WF1) - \delta(F4WF3) + \delta(SWF5)$
			201 (<1) [0]	$\nu_7(B_1)$, $\delta_{out\text{-}of\text{-}plane}(WF_{4,eq})$
131 (19)			117 (1) [<1]	$\nu_{11}(E)$, $\delta(F2WF1) - \delta(F4WF3) + \rho(SWF5)$
97 sh				
71 (32)				lattice modes
59 (44)				

[a]Abbreviations denote shoulder (sh), very strong (vs), strong (s), medium (m), and broad (br). [b]Relative intensities are given in parentheses. The $N(CH_3)_4^+$ cation modes were observed in the Raman spectrum at 458 (8), $\nu_{19}(T_2)$; 740 sh, 753 (31), $\nu_3(A_1)$; 948 (22), 983 (4), $\nu_{18}(T_2)$; 1420 (8), $\nu_{16}(T_2)$; 1461 (24), $\nu_2(A_1)$, $\nu_6(E)$; 2820 (12), 2927 (24), 2960 (28), 2986 (40), 3040 (36) cm^{-1}, $\nu(CH_3)$ and binary bands; bands for an impurity of the $W_2S_2F_9^-$ anion were observed at 679 (8), 556 (22), and 241 (14) cm^{-1}; a laser line was observed at 84 cm^{-1}. [c]Unscaled Raman intensities, in $Å^4\ u^{-1}$, are given in parentheses; IR intensities, in km mol^{-1}, are given in square brackets. [d]The $N(CH_3)_4^+$ cation modes were observed in the IR spectrum at 457 w, $\nu_{19}(T_2)$; 949 vs, 957 vs, $\nu_{18}(T_2)$; 1252 w, $\nu_{17}(T_2)$; 1488 vs, 1497 vs, $\nu_{15}(T_2)$; 2921 w, 2962 w, 3034 s cm^{-1}, ν_{CH_3} and binary bands. [e]Values are from ref 5.

The small number of bands associated with the $W_2S_2F_9^-$ anion and observed by Raman and IR spectroscopy is in accordance with the very few modes that are predicted to have sufficiently large intensities observable in the recorded frequency ranges. The bands at 560 and 556 cm^{-1} in the Raman spectrum and at 578 and 553 cm^{-1} in the IR spectrum are attributed to the in-phase and out-of-phase combinations of the two W−S stretching vibrations, respectively, and are closer to the stretching frequency of monomeric WSF_4 than that of the WSF_5^- anion, reflecting the lower overall charge density and more covalent W═S bonding in the dinuclear anion compared to the mononuclear anion. The calculated values predict similar frequencies for the in-phase (541 cm^{-1}) and out-of-phase (535 cm^{-1}) ν(W−S) stretching modes, which is likely a consequence of the overestimated $W-F_{br}$ distance in the calculations, resulting in weaker vibrational coupling between the two WSF_4 moieties. The most intense W−F stretching bands in the Raman spectrum appear at 672 and 678 cm^{-1} and are assigned to the in-phase combination of the two $\nu_s(WF_4)$ vibrations. The intense, high-frequency W−F stretching band in the IR spectrum at 688 cm^{-1} is assigned to the out-of-phase combination of the two $\nu_s(WF_4)$ vibrations. Both are significantly higher than $\nu_s(WF_5)$ of the WSF_5^- anion at 664 cm^{-1}, reflecting less ionic bonding in the dinuclear anion compared to the mononuclear anion. The calculated values (B3LYP: in-phase, 686 cm^{-1}; out-of-phase, 688 cm^{-1}) are in very good agreement with the observed values. The most intense IR band at 625 cm^{-1} is assigned to the two in-phase combinations of the two $\nu_{as}(WF_4)$ vibrations, which are calculated to be degenerate in the linear geometry. The corresponding $\nu_{as}(WF_4)$ mode of the WSF_5^- anion (598 cm^{-1}) also appears at a lower frequency than that observed for the dinuclear anion. The strong band observed at 434 cm^{-1} in the IR spectrum is associated with the $W-F_b$ stretching modes and appears at slightly higher frequency than the calculated frequency (403 cm^{-1}). All deformation modes are calculated to have frequencies below 306 cm^{-1}, and therefore none of them was observed in the IR spectrum. However, the two bending modes that are predicted to be strong enough to be observed in the Raman spectrum were observed at 243 and 298 cm^{-1}, in agreement with the calculated values, 237 and 241 cm^{-1}. The bending mode at 243 cm^{-1} is assigned to the out-of-phase combination of the umbrella motions of the two WF_4 groups, whereas the band at 298 cm^{-1} is attributed to a S−W−F bending mode.

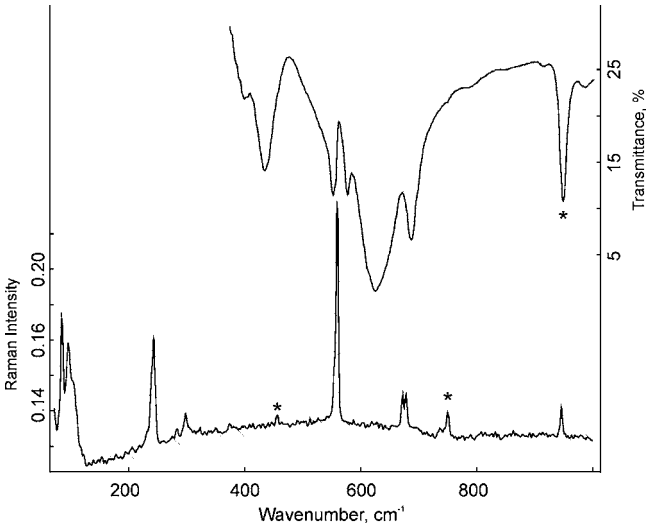

Figure 2. Vibrational spectra of $[N(CH_3)_4][W_2S_2F_9]$: IR spectrum (upper trace) recorded at room temperature as a KBr pellet and Raman spectrum recorded at −100 °C using 1064-nm excitation. Asterisks (*) denote $N(CH_3)_4^+$ cation bands.

NMR Spectroscopy. The tetramethylammonium salts of WSF_5^- and $W_2S_2F_9^-$ were studied in CH_3CN solvent by ^{19}F NMR spectroscopy. In a sample of $[N(CH_3)_4][W_2S_2F_9]$ in CH_3CN, the $W_2OSF_9^-$ anion was observed for the first time by ^{19}F NMR spectroscopy. The ^{19}F NMR parameters for these anions are given in Table 3.

As expected, the equatorial and axial fluorine environments in the WSF_5^- anion give rise to a doublet and a quintet with ^{183}W satellites at 77.2 and −111.4 ppm, respectively. These chemical shift values differ from some of the previously reported values for the axial[5] and equatorial[3,4] fluorine environments observed in the same, except deuterated, solvent. The absolute value of the ^1J ($^{19}F_{eq}-^{183}W$) coupling constant is found to be significantly smaller than that of $|^1J(^{19}F_{ax}-^{183}W)|$,

dx.doi.org/10.1021/ic3005882 | Inorg. Chem. 2012, 51, 6350−6359

Table 2. Observed and Calculated Vibrational Frequencies for $W_2S_2F_9^-$ and Their Assignments

exptl[a]		calcd[b]		
Raman[c]	IR[d]	bent	linear	assignment (C_1)
	688 s	688 (<1) [172]	679 (<0.1) [184]	$\nu(WF_{1-4}) - \nu(W'F_{1-4}')$
678 (13)		686 (31) [<1]	676 (32) [<0.1]	$\nu(WF_{1-4}) + \nu(W'F_{1-4}')$
672 (13)	625 vs	664 (<1) [407]	650 (<0.1) [425]	$[\nu(WF_1) - \nu(WF_3)] + [\nu(W'F_1') - \nu(W'F_3')]$
		659 (<0.1) [400]	650 (<0.1) [425]	$[\nu(WF_2) - \nu(WF_4)] + [\nu(W'F_2') - \nu(W'F_4')]$
		646 (<1) [44]	634 (<1) [<0.1]	$[\nu(WF_1) - \nu(WF_3)] + [\nu(W'F_3') - \nu(W'F_1')]$
		641 (<1) [5]	634 (<1) [<0.1]	$[\nu(WF_2) - \nu(WF_4)] + [\nu(W'F_4') - \nu(W'F_2')]$
		609 (3) [<1]	601 (3) [<0.1]	$([\nu(WF_1) + \nu(WF_3)] - [\nu(WF_2) + \nu(WF_4)]) + ([\nu(W'F_2') + \nu(W'F_4')] - [\nu(W'F_1') + \nu(W'F_3')])_{small}$
		609 (3) [1]	600 (3) [<0.1]	$([\nu(WF_1) + \nu(WF_3)] - [\nu(WF_2) + \nu(WF_4)])_{small} + ([\nu(W'F_2') + \nu(W'F_4')] - [\nu(W'F_1') + \nu(W'F_3')])$
560 (100)	578 m	541 (120) [6]	539 (124) [<0.1]	$\nu(WS) + \nu(W'S')$
556 sh	553 m	535 (2) [174]	533 (<0.1) [167]	$[\nu(WS) - \nu(W'S')] + [\nu(WF_{br}) - \nu(W'F_{br})]_{small}$
	434 s	403 (1) [457]	410 (<0.1) [503]	$\nu(WF_{br}) - \nu(W'F_{br})$
		306 (<1) [7]	297 (2) [<0.1]	$[\delta(F_1WF_4) + \delta(F_2WF_3)] + [\delta(F_1'W'F_4') + \delta(F_2'W'F_3')]$
		301 (1) [<1]	296 (1) [<0.1]	$[\delta(F_1WF_4) + \delta(F_2WF_3)] - [\delta(F_1'W'F_4') + \delta(F_2'W'F_3')]$
		301 (1) [<0.1]	294 (<0.1) [6]	$[\rho_w(F_1WF_2) - \rho_w(F_3WF_4)] + [\delta(F_1'W'F_{br}) - \delta(F_3'W'F_{br})]$
		292 (<0.1) [6]	294 (<0.1) [6]	$[\rho_w(F_2WF_3) - \rho_w(F_1WF_4)] + [\delta(F_2'W'F_{br}) - \delta(F_4'W'F_{br})]$
		277 (<1) [<1]	274 (1) [<0.1]	$\delta(WF_{1-4})_{umb} + \delta(W'F_{1-4}')_{umb}$
298 (10)		241 (5) [48]	237 (8) [<0.1]	$\delta(SWF_3) - \delta(S'W'F_3')$
		238 (1) [182]	234 (<0.1) [245]	$[\delta(SWF_2) - \delta(SWF_4)] + [\delta(S'W'F_4') - \delta(S'W'F_2')]$
243 (40)		237 (8) [<1]	237 (8) [<0.1]	$\delta(WF_{1-4})_{umb} - \delta(W'F_{1-4}')_{umb}$
		229 (<1) [22]	224 (<0.1) [24]	$[\delta(WSF_1F_2) - \delta(F_3WF_4)] + [\delta(W'S'F_3'F_4') - \delta(F_1'W'F_2')]$
		227 (<0.1) [28]	224 (<0.1) [24]	$\delta(WSF_2F_4) - \delta(W'S'F_2'F_4')$
		217 (<1) [<0.1]	211 (<0.1) [<0.1]	$\rho_w(F_1WF_3) - \rho_w(F_1'W'F_3')$
		215 (<0.1) [<1]	211 (<0.1) [<0.1]	$\rho_w(F_2WF_4) - \rho_w(F_2'W'F_4')$
		189 (<1) [<0.1]	187 (<1) [<0.1]	$\rho_w(F_1WF_3) - \rho_w(F_2W'F_4)$
		189 (<1) [3]	187 (<1) [<0.1]	$\rho_w(F_1'W'F_3') - \rho_w(F_2'W'F_4')$
		173 (<1) [1]	156 (1) [<0.1]	$[\delta(SWF_{br}) - \delta(F_2WF_4)] + [\delta(F_{br}W'S') - \delta(F_2'W'F_4')]$
		157 (<1) [<1]	156 (1) [<0.1]	$[\delta(SWF_{br}) - \delta(F_1WF_3)] + [\delta(F_{br}W'S') - \delta(F_1'W'F_3')]$
		95 (<1) [<0.1]	96 (<1) [<0.1]	$\rho_w(SWF_{1-4}) + \rho_w(S'W'F_{1-4}')$
		89 (5) [<1]	85 (5) [0]	$\rho_r(SWF_1F_3) + \rho_r(S'W'F_1'F_3')$
		86 (5) [<0.1]	85 (5) [0]	$\rho_r(SWF_2F_4) + \rho_r(S'W'F_2'F_4')$
		47 (<1) [<1]	16 (0) [<1]	$\rho_r(WF_{1-4}) - \rho_r(W'F_{1-4}')$
		44 (<0.1) [<0.1]	15 (0) [<1]	$\delta(WF_{br}W')$
		−21 (<0.1) [<1]	11 (0) [<0.1]	$\rho_t(WSF_2F_4) - \rho_t(W'S'F_2'F_4')$

[a]Abbreviations denote shoulder (sh), very strong (vs), strong (s), medium (m), weak (w), and very weak (vw). [b]The B3LYP level of theory. IR intensities, in km mol^{-1}, are given in parentheses; Raman intensities, in $Å^4$ u^{-1}, are given in square brackets. [c]The $N(CH_3)_4^+$ cation modes were observed in the Raman spectrum (−100 °C) at 457 (4), $\nu_{19}(T_2)$; 751 (11), $\nu_3(A_1)$; 947, $\nu_{18}(T_2)$; 1454 (13), $\nu_2(A_1)$; 2924 (9), 2990 (18), 3043 (12) cm^{-1}, ν_{CH3} and binary bands. [d]The $N(CH_3)_4^+$ cation modes were observed in the IR spectrum at 949 s, 988 w, $\nu_{18}(T_2)$; 1265 w, $\nu_{17}(T_2)$; 1420 w, $\nu_{16}(T_2)$; 1486 vs, $\nu_{15}(T_2)$; 2929 w, 2971 w, 3052 w cm^{-1}, ν_{CH_3} and binary bands. An impurity of WOF_5^- was observed at 1022 cm^{-1} (small), ν(WO).

Table 3. ^{19}F NMR Spectroscopic Data for the $N(CH_3)_4^+$ Salts of WSF_5^-, $W_2S_2F_9^-$, and $W_2OSF_9^-$ in CH_3CN Solvent at Room Temperature

	$\delta(^{19}F)$,[a] ppm	$^1J(^{183}W-^{19}F)$, Hz	$^2J(^{19}F-^{19}F)$, Hz
WSF_5^-	77.2 (d) (F_{eq})	28.3	75.5
	−111.4 (qn) (F_{ax})	68.6	
$W_2S_2F_9^-$ [b]	85.6 (d) (F_{term})	31.3	70.0
	−156.5 (n) (F_{br})	83.9	
$W_2OSF_9^-$ [b]	86.0 (d) ($F_{term, W=S}$)	16−19[c]	70.3
	60.8 (d) ($F_{term, W=O}$)	71.0	56.7
	−148.1 (qn/qn) (F_{br})	not obsd	

[a]Abbreviations denote doublet (d), quintet (qn), nonet (n), and quintet of quintets (qn/qn). [b]Signals were observed for $WSF_4{\cdot}CH_3CN$ [singlet at 85.4 ppm, satellites, $^1J(^{183}W-^{19}F)$ = 33.4 Hz], WOF_5^- [doublet at 48.4 ppm, $^2J(^{19}F-^{19}F)$ = 51.9 Hz, quintet at −83.5 ppm], and WSF_5^-. [c]Uncertainty arises from an overlap with the ^{19}F NMR resonance for $W_2S_2F_9^-$.

although the $W-F_{eq}$ bond is stronger and less ionic than the $W-F_{ax}$ bond. This counterintuitive finding can be explained by assuming that the two J values have different signs based on the previous determination of opposite signs of the axial and equatorial $^1J(^{19}F-^{183}W)$ coupling constants for the related WOF_5^- anion by homonuclear ^{19}F tickling experiments.[11] The opposite signs of the axial and equatorial J values in WOF_5^- and WSF_5^- can only be the result of dramatically different contributions of at least two different scalar coupling mechanisms of opposite sign. As a consequence, a simple correlation between the bond length and the absolute values of the J coupling constants cannot be made.

The present ^{19}F NMR data for the $W_2S_2F_9^-$ anion in CH_3CN solvent [doublet, $\delta(^{19}F_{term})$ = 85.6 ppm; nonet, $\delta(^{19}F_{br})$ = −156.5 ppm; Figure 3] are in excellent agreement with those reported in the literature.[3,4] In addition, the present NMR study could resolve the $^1J(^{19}F-^{183}W)$ coupling constants for the first time for the terminal (31.3 Hz) and bridging (83.9 Hz) fluorine environments. The larger $|^1J(^{19}F-^{183}W)|$ coupling

dx.doi.org/10.1021/ic3005882 | Inorg. Chem. 2012, 51, 6350−6359

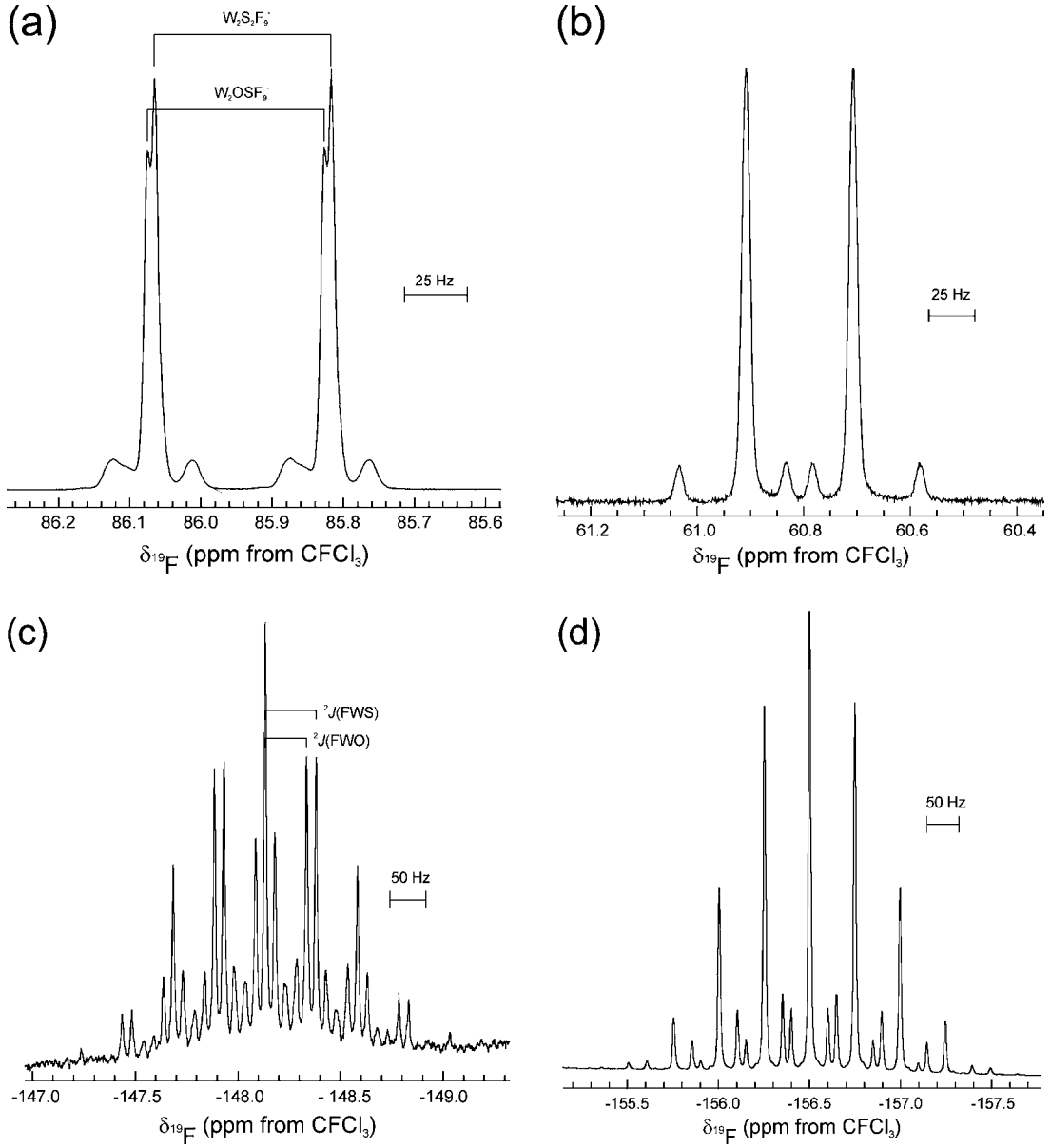

Figure 3. ^{19}F NMR spectrum of $[N(CH_3)_4][W_2S_2F_9]$ in CH_3CN solvent at ambient temperature, including the $[N(CH_3)_4][W_2OSF_9]$ impurity: (a) terminal fluorine environments of $W_2S_2F_9^-$ and the WSF_4 moiety of $W_2OSF_9^-$; (b) terminal fluorine environment of WOF_4 moiety of $W_2OSF_9^-$; (c) bridging fluorine environment of $W_2OSF_9^-$ [$^2J(^{19}F_t-^{19}F_{br})$ couplings are indicated]; (d) bridging fluorine environment of $W_2S_2F_9^-$.

constant for the weaker and more ionic W---F_{br} bond compared to that of the terminal W−F bond is unexpected but can also be explained by assuming different contributions of at least two different J coupling mechanisms of opposite sign, resulting in opposite signs of the terminal and bridging J coupling values. As for the axial and equatorial fluorine environments in the WOF_5^- anion, the $^1J(^{19}F_{term}-^{183}W)$ and $^1J(^{19}F_{br}-^{183}W)$ values for the $W_2O_2F_9^-$ anions have been shown to have opposite signs by homonuclear ^{19}F tickling experiments.[11]

In the ^{19}F NMR spectra of $[N(CH_3)_4][W_2S_2F_9]$, additional signals were observed that could not be attributed to known compounds. The new signals, i.e., two doublets and a quintet of quintets, can be assigned to the novel $W_2OSF_9^-$ anion (Figure 3), which had formed as a result of accidental hydrolysis and which was subsequently generated in an admixture with sulfide fluoride and oxide fluoride species (vide supra) by deliberate synthetic routes. The doublet at 86.0 ppm can be assigned to the terminal fluorine environments of the WSF_4 moiety because its chemical shift is only slightly higher than that of the terminal fluorines in $W_2S_2F_9^-$. The lower frequency doublet at 60.8 ppm arises from the terminal fluorine environments of the WOF_4 moiety, which is similar to the chemical shift of the terminal fluorine environment of $W_2O_2F_9^-$ (61.8 ppm). The bridging fluorine appears, as expected, at low frequency between those of the $W_2O_2F_9^-$ and $W_2S_2F_9^-$ anions. The coupling of the bridging fluorine to the two nonequivalent terminal fluorine environments results in a quintet of quintets with two different $^2J(^{19}F-^{19}F)$ coupling values that are in the characteristic ranges for tungsten(VI) oxide fluorides and sulfide fluorides. The anion is the first anion with bridged oxide fluoride and sulfide fluoride moieties. Attempts to isolate a pure salt of this mixed oxide sulfide anion have been unsuccessful so far because of equilibria operative between this dinuclear anion and the mononuclear species.

dx.doi.org/10.1021/ic3005882 | *Inorg. Chem.* 2012, 51, 6350−6359

Crystal Structures of $[N(CH_3)_4][WSF_5]\cdot CH_3CN$ and $[N(CH_3)_4][W_2S_2F_9]$. Details of the data collection parameters and other crystallographic information for $[N(CH_3)_4][WSF_5]\cdot CH_3CN$ and $[N(CH_3)_4][W_2S_2F_9]$ are given in Table 4, while important bond lengths and angles are listed in Tables 5 and 6, respectively.

Table 4. Crystallographic Data for $[N(CH_3)_4][WSF_5]\cdot CH_3CN$ and $[N(CH_3)_4][W_2S_2F_9]$

chemical formula	$C_6H_{15}F_5N_2SW$	$C_4H_{12}F_9NS_2W_2$
space group	$P2_1/c$	$Pnma$
a (Å)	7.7095(11)	13.122(2)
b (Å)	19.815(3)	7.8937(12)
c (Å)	8.1597(12)	14.072(2)
β (deg)	90.562(2)	90
molecules/unit cell	4	4
mol wt (g mol^{-1})	426.11	676.97
calcd density (g cm^{-3})	2.271	3.085
T (°C)	−155	−130
μ (mm^{-1})	9.469	16.136
R1[a]	0.0415	0.0244
wR2[b]	0.1089	0.0581

[a] R1 is defined as $\sum||F_o| - |F_c||/\sum|F_o|$ for $I > 2\sigma(I)$. [b] wR2 is defined as $[\sum[w(F_o^2 - F_c^2)^2]/\sum w(F_o^2)^2]^{1/2}$ for $I > 2\sigma(I)$.

Table 5. Experimental and Calculated Metric Parameters for the WSF_5^- Anion

	exptl	calcd
	Bond Lengths (Å)	
W–S	2.114(2)	2.184
W–F(1)	1.871(5)	1.894
W–F(2)	1.870(5)	1.894
W–F(3)	1.884(4)	1.894
W–F(4)	1.880(4)	1.894
W–F(5)	1.998(5)	1.964
	Bond Angles (deg)	
S–W–F(1)	97.70(16)	96.2
S–W–F(2)	96.82(15)	96.2
S–W–F(3)	96.80(17)	96.2
S–W–F(4)	97.32(17)	96.2
S–W–F(5)	179.72(14)	180.0
F(1)–W–F(2)	89.4(3)	89.3
F(1)–W–F(3)	165.5(2)	167.6
F(1)–W–F(4)	89.7(2)	89.3
F(1)–W–F(5)	82.50(19)	83.8
F(2)–W–F(3)	89.5(2)	89.3
F(2)–W–F(4)	165.8(2)	167.6
F(2)–W–F(5)	82.99(19)	83.8
F(3)–W(2)–F(4)	88.0(2)	89.3
F(3)–W(2)–F(5)	83.0(2)	83.8
F(4)–W(2)–F(5)	82.9(2)	83.8

$[N(CH_3)_4][WSF_5]\cdot CH_3CN$. The $[N(CH_3)_4][WSF_5]\cdot CH_3CN$ salt crystallizes from a solution of $[N(CH_3)_4][WSF_5]$ in CH_3CN in the monoclinic space group $P2_1/c$ with one crystallographically independent formula unit in the unit cell. The crystal structure contains well-separated $N(CH_3)_4^+$ cations, WSF_5^- anions, and CH_3CN solvent molecules. Interestingly, one CH_3CN solvent molecule cocrystallizes with the $[N(CH_3)_4][WSF_5]$ salt, as observed in the crystal structure of $[\{(C_6H_5)_3P\}_2N][WSF_5]\cdot CH_3CN$,[5] although no significant

Table 6. Experimental and Calculated Metric Parameters for the Staggered $W_2S_2F_9^-$ Anion

exptl		calcd	
	Bond Lengths (Å)		
W(2)–S(2)	2.0981(6)	W–S	2.146
W(2)–F(6)	1.8525(14)	W–F_3	1.874
W(2)–F(7A)	1.8568(13)	W–F_4	1.875
W(2)–F(8)	1.8482(15)	W–F_1	1.876
W(2)–F(7)	1.8569(13)	W–F_2	1.877
W(2)–F(5)	2.1324(13)	W–F_b	2.157
W(1)–S(1)	2.0955(7)	W′–S′	2.146
W(1)–F(1A)	1.8649(11)	W′–F_2′	1.874
W(1)–F(1)	1.8649(11)	W′–F_3′	1.874
W(1)–F(3A)	1.8589(10)	W′–F_4′	1.877
W(1)–F(3)	1.8589(10)	W′–F_1′	1.877
W(1)–F(5)	2.1246(13)	W′–F_b	2.157
	Bond Angles (deg)		
S(2)–W(2)–F(6)	100.22(5)	S–W–F_3	99.0
S(2)–W(2)–F(7A)	99.65(4)	S–W–F_4	98.8
S(2)–W(2)–F(8)	98.74(6)	S–W–F_1	99.0
S(2)–W(2)–F(7)	99.65(4)	S–W–F_2	98.8
S(2)–W(2)–F(5)	177.36(4)	S–W–F_b	179.6
F(6)–W(2)–F(7A)	87.06(4)	F_3–W–F_4	88.9
F(6)–W(2)–F(8)	161.05(7)	F_3–W–F_1	162.0
F(6)–W(2)–F(7)	87.06(4)	F_3–W–F_2	88.4
F(6)–W(2)–F(5)	82.42(6)	F_3–W–F_b	81.1
F(7A)–W(2)–F(6)	87.06(4)	F_4–W–F_1	88.7
F(7A)–W(2)–F(7)	160.54(8)	F_4–W–F_2	162.3
F(7A)–W(2)–F(5)	80.42(4)	F_4–W–F_b	80.7
F(8)–W(2)–F(7A)	89.78(4)	F_1–W–F_2	88.4
F(8)–W(2)–F(5)	78.63(6)	F_1–W–F_b	80.9
F(7)–W(2)–F(5)	80.42(4)	F_2–W–F_b	81.6
S(1)–W(1)–F(5)	177.99(4)	S′–W′–F_b	179.6
S(1)–W(1)–F(1)	99.18(4)	S′–W′–F_3′	99.0
S(1)–W(1)–F(3A)	98.56(3)	S′–W′–F_4′	98.8
S(1)–W(1)–F(3)	98.56(3)	S′–W′–F_1′	99.0
S(1)–W(1)–F(1A)	99.18(4)	S′–W′–F_2′	98.9
F(1)–W(1)–F(5)	82.26(4)	F_3′–W′–F_b	81.1
F(1)–W(1)–F(3A)	88.79(5)	F_3′–W′–F_4′	88.4
F(1)–W(1)–F(3)	162.22(5)	F_3′–W′–F_1′	162.0
F(1A)–W(1)–F(1)	87.18(7)	F_2′–W′–F_3′	88.9
F(3A)–W(1)–F(5)	80.04(4)	F_4′–W′–F_b	81.6
F(3A)–W(1)–F(3)	89.79(5)	F_4′–W′–F_1′	88.4
F(1A)–W(1)–F(3A)	162.22(5)	F_2′–W′–F_4′	162.3
F(3)–W(1)–F(5)	80.04(4)	F_1′–W′–F_b	80.9
F(1A)–W(1)–F(3)	88.79(5)	F_2′–W′–F_1′	88.7
F(1A)–W(1)–F(5)	82.26(4)	F_2′–W′–F_b	80.7
W(1)–F(5)–W(2)	151.56(7)	W–F_b–W′	159.3

interactions between CH_3CN and the anions or cations are found in both cases. The packing of $[N(CH_3)_4][WSF_5]\cdot CH_3CN$ is comprised of layers of $N(CH_3)_4^+$ cations in the *ac* plane, separating layers of WSF_5^-/CH_3CN (Figure S3 in the Supporting Information).

The WSF_5^- anion (Figure 4) adopts a pseudooctahedral geometry similar to that observed in $[\{(C_6H_5)_3P\}_2N][WSF_5]\cdot CH_3CN$. In the $N(CH_3)_4^+$ salt, the W–F_{eq} bonds cis to the W=S bond range from 1.870(5) to 1.884(4) Å and are significantly shorter than the W–F_{ax} bond trans to W=S [1.998(5) Å], as a consequence of the trans influence of the W=S bond. The W=S bond length in $[N(CH_3)_4][WSF_5]\cdot CH_3CN$ [2.114(2) Å] is somewhat shorter than that

dx.doi.org/10.1021/ic3005882 | Inorg. Chem. 2012, 51, 6350–6359

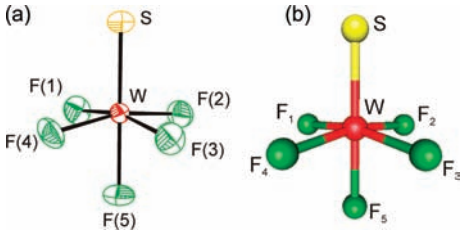

Figure 4. Views of the WSF_5^- anion: (a) thermal ellipsoid plot of the WSF_5^- anion in the crystal structure of $[N(CH_3)_4][WSF_5]\cdot CH_3CN$ (thermal ellipsoids are drawn at the 50% probability level); (b) optimized geometry of WSF_5^- in the gas phase.

observed for $[\{(C_6H_5)_3P\}_2N][WSF_5]\cdot CH_3CN$ [2.123(1) Å], and as a result, the W−F_{ax} bond in the $N(CH_3)_4^+$ salt is elongated compared to that in the $\{(C_6H_5)_3P\}_2N^+$ salt. In both crystal structures, the S−W−F_{ax} moiety is essentially linear and the S−W−F_{eq} angles in both salts are comparable.

$[N(CH_3)_4][W_2S_2F_9]$. The $[N(CH_3)_4][W_2S_2F_9]$ salt crystallized from a solution of $[N(CH_3)_4][WSF_5]$ in aHF in the orthorhombic space group *Pnma*. The crystal structure contains well-separated dinuclear fluorine-bridged $W_2S_2F_9^-$ anions and $N(CH_3)_4^+$ cations.

The W−S [2.0981(6) and 2.0955(7) Å] and terminal W−F [1.8482(15) to 1.8649(11) Å] bond lengths in the $W_2S_2F_9^-$ anion (Figure 5) are significantly shorter than those observed for the WSF_5^- anion, reflecting the lower charge density and the more covalent bonding in the dinuclear anion. This finding corroborates the higher W═S and W−F stretching frequencies observed for the dinuclear anion compared to those of the mononuclear anion. The bridging fluorine is close to being symmetric, with W−F_{br} distances of 2.1324(13) and 2.1246(13) Å. These distances are significantly longer than the W−F_{ax} bond in the WSF_5^- anion. The W−F_{br}−W angle is bent [151.56(7)°]. The two WF_4 moieties adopt a staggered conformation, and the S−W−F_{br} angles deviate slightly from linearity. The W−F_{br}−W angle is expected to be somewhat flexible and dependent on the packing in the crystal lattice. Within experimental error, the W−F_{br}−W angle is slightly larger than that observed in the related $W_2O_2F_9^-$ anion in the crystal structure of $[H_3O][W_2O_2F_9]$ [144(2)°]. Similar to the $W_2S_2F_9^-$ anion, the two WOF_4 moieties are staggered with respect to each other. The calculated W−F_{br}−W angle of the gas-phase geometry is somewhat larger (159.3°) than the experimental value.

Computational Results. The electronic structures of the WSF_5^- and $W_2S_2F_9^-$ anions in the gas phase were optimized at the B3LYP level and resulted in stationary points with all frequencies real, except for the staggered/bent and linear/eclipsed geometries of the $W_2S_2F_9^-$ anion, which resulted in local minima with one negative frequency. The optimized geometries of the WSF_5^- and $W_2S_2F_9^-$ anions are depicted in Figures 4 and 5, respectively, and the calculated metric parameters are listed in Tables 5 and 6, respectively. The same level of theory has previously been employed for WSF_4 and its nitrogen-base adducts and produced excellent agreement with experimental findings.[1,2] Attempts to optimize the geometry of the novel $W_2SOF_9^-$ anion did not yield an energy minimum.

a. Calculated Geometries. The geometry optimization of WSF_5^- in the gas phase resulted in a C_{4v} geometry, with the calculated W═S and W−F_{eq} bond lengths being somewhat longer than the experimental ones. The calculated W−F_{ax} bond

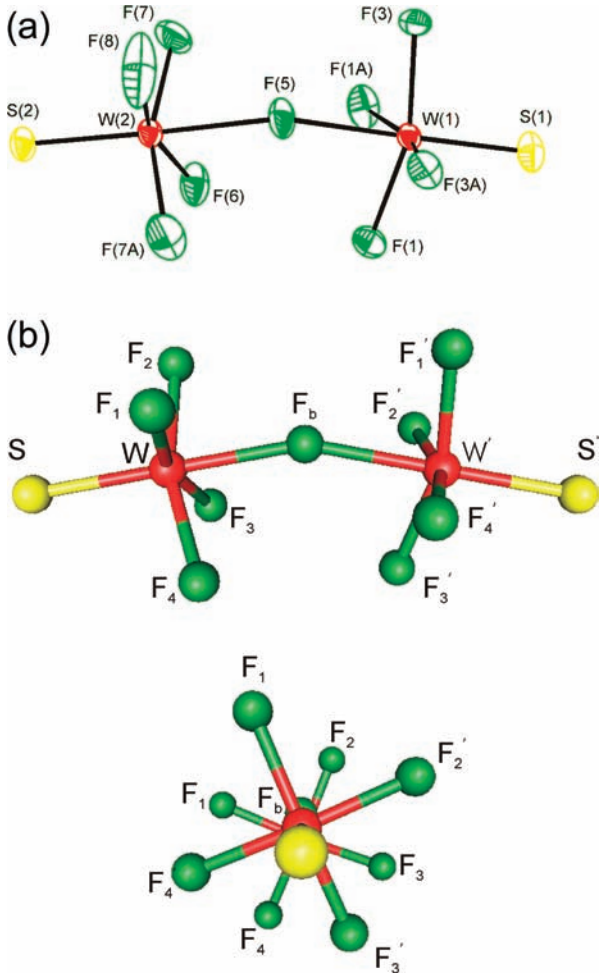

Figure 5. Views of the $W_2S_2F_9^-$ anion: (a) thermal ellipsoid plot of the $W_2S_2F_9^-$ anion in the crystal structure of $[N(CH_3)_4][W_2S_2F_9]$ (thermal ellipsoids are drawn at the 50% probability level); (b) optimized geometry of $W_2S_2F_9^-$ in the gas phase.

length (1.964 Å), on the other hand, is underestimated compared to the experimental value [1.998(5) Å].

The three conformations of the $W_2S_2F_9^-$ anion that gave local minima have very similar energies, with the bent/staggered geometry (also the experimental geometry) being more stable than the linear/eclipsed and linear/staggered conformations by only 1.88 and 3.97 kJ mol^{-1}. These results confirm that the geometry of the anion will easily be affected by packing effects in the solid state. In the optimized bent/staggered geometry, all W═S and W−F bond lengths are somewhat larger compared to the experimental values, which is expected because ion pairing is not taken into account in the calculated gas-phase geometry. Ion pairing in the solid state will reduce the negative charge of the anion, resulting in less polar W═S and W−F bonds.

b. Vibrational Frequencies. The calculated vibrational frequencies for the WSF_5^- and $W_2S_2F_9^-$ anions are listed in Tables 1 and 2. The experimental and calculated vibrational frequencies for WSF_5^- are in good agreement. Overall, the frequencies for the bent and linear staggered geometries of the $W_2S_2F_9^-$ anion are comparable, with those associated with the linear conformation coming at slightly lower frequency. As expected, the largest difference occurs for δ(W−F_{br}−W′), which

dx.doi.org/10.1021/ic3005882 | *Inorg. Chem.* 2012, 51, 6350−6359

occur at 15 and 44 cm^{-1} for the linear and bent configurations, respectively.

c. Charges, Valencies, and Bond Orders. Natural bond order (NBO) analyses were carried out at the B3LYP level of theory for the WSF_5^-, bent $W_2S_2F_9^-$, and linear $W_2S_2F_9^-$ anions. The natural population analysis (NPA) charges, the valencies, and bond orders are listed in Table 7. The axial

Table 7. NBO Valencies, Bond Orders, and NPA Charges for WSF_5^- and $W_2S_2F_9^-$ (Bent and Linear Geometries)

	WSF_5^-		$W_2S_2F_9^-$ (bent)		$W_2S_2F_9^-$ (linear)	
	charges	valencies	charges	valencies	charges	valencies
W	2.129	3.717	2.099	3.617	2.100	3.617
S	−0.372	1.112	−0.237	1.182	−0.236	1.180
F_1	−0.535	0.544	−0.510	0.563	−0.508	0.565
F_2	−0.535	0.544	−0.510	0.562	−0.508	0.565
F_3	−0.535	0.544	−0.504	0.570	−0.508	0.564
F_4	−0.535	0.544	−0.506	0.567	−0.508	0.564
F_5	−0.617	0.432	−0.664	0.481	−0.665	0.483

	bond orders		
	WSF_5^-	$W_2S_2F_9^-$ (bent)	$W_2S_2F_9^-$ (linear)
W−S	1.129	1.183	1.181
W−F_1	0.539	0.551	0.552
W−F_2	0.539	0.550	0.552
W−F_3	0.539	0.554	0.552
W−F_4	0.539	0.553	0.552
W−F_5	0.431	0.230	0.231

fluorine in WSF_5^-, and more so the bridging fluorine $W_2S_2F_9^-$, bear the largest negative charge, reflecting the more ionic W−F_{ax} and W−F_{br} bonding compared to bonding to the equatorial and terminal fluorine atoms. The W═S bond order in these anions is more than double the W−F_{eq} and F_{term} bond orders, while the bonds to the axial and bridging fluorine atoms are significantly weaker than those to the equatorial and terminal fluorine atoms in WSF_5^- and $W_2S_2F_9^-$, respectively.

CONCLUSIONS

The fluoride-ion acceptor properties of WSF_4 have been studied. While one aliquot of F^- yields the WSF_5^- anion, half an aliquot produces the dinuclear $W_2S_2F_9^-$ anion. Tetramethylammonium salts of these anions were isolated and characterized by Raman and IR spectroscopy in the solid state and ^{19}F NMR spectroscopy in solution. Metric parameters were obtained for both anions from crystal structures. The fluoride-ion addition to WSF_4 represents a new synthetic route to salts of these anions, and the $W_2S_2F_9^-$ anion was characterized in the solid state for the first time. The $[N(CH_3)_4][SSi(CH_3)_3]$ reagent was prepared and its utility as a sulfide-transfer agent was shown in the reaction with WF_6, providing an alternative route to $[N(CH_3)_4][WSF_5]$. Fluorine-19 NMR spectroscopic characterization of $W_2SOF_9^-$ in solution provided evidence for the first fluorine-bridged tungsten oxide fluoride and sulfide fluoride species.

EXPERIMENTAL SECTION

Materials and Apparatus. All volatile materials were handled on a Pyrex vacuum line equipped with glass/Teflon J. Young valves. Nonvolatile materials were handled in the dry nitrogen atmosphere of a drybox (Omni Lab, Vacuum Atmospheres).

Acetonitrile solvent (Baker, HPLC grade) was purified according to the standard literature method.[13] The syntheses of WSF_4,[1] anhydrous $[N(CH_3)_4]F$,[8] and WOF_4[13] have been described previously.

Elemental analyses were performed using an Elementar Vario Microcube instrument.

Preparation of $[N(CH_3)_4][SSi(CH_3)_3]$. Inside the drybox, 0.099 g (1.1 mmol) of anhydrous $[N(CH_3)_4]F$ was loaded into the side arm of a two-armed glass vessel equipped with a J. Young stopcock. Excess $S(Si(CH_3)_3)_2$ (0.280 g, 1.57 mmol) was vacuum distilled into the straight arm of the glass vessel, followed by vacuum distillation of approximately 1 mL of CH_3CN into both arms. The solutions were combined at −35 °C, instantaneously yielding a white precipitate. After agitation for ca. 15 min at −30 °C, volatiles were removed under dynamic vacuum, first at low temperature, followed by pumping at ambient temperatures, yielding a finely divided white solid (collected yield: 0.153 g, 8.53 mmol). Decomposition at 191 °C. ^1H NMR (CH_3CN, unlocked, 300.13 MHz, δ [ppm]): 3.35 (s, $N(CH_3)_4^+$), 0.16 (s, $(CH_3)_3SiS^-$). $^{13}C\{^1H\}$ NMR (CH_3CN, unlocked, 100.61 MHz, δ [ppm]): 55.73 (t, $^1J(^{14}N-^{13}C)$ = 4.1 Hz, $N(CH_3)_4^+$), 8.44 (s, $(CH_3)_3SiS^-$). Anal. Found: C, 46.69; H, 11.95; N, 8.12. Anal. Calcd for $C_7H_{21}NSSi$: C, 46.90; H, 11.82; N, 7.82.

Preparation of $[N(CH_3)_4][WSF_5]$. (a) Inside the drybox, 0.136 g (0.466 mmol) of WSF_4 and 0.042 g (0.45 mmol) of $[N(CH_3)_4][F]$ were loaded into a $^1/_4$-in.-o.d. FEP reactor equipped with a Kel-F valve. After vacuum distillation of 0.5 mL of CH_3CN onto the solid, agitation at −35 °C resulted in a yellow solution above a dark-brown solid. Removal of volatiles yielded 0.178 g of beige $[N(CH_3)_4][WSF_5]$. Decomposition at 133 °C. Anal. Found: C, 12.48; H, 2.84; N, 3.99. Anal. Calcd for $C_4H_{12}F_5NSW$: C, 11.48; H, 3.14; N, 3.64.

(b) Inside the drybox, 0.026 g (0.15 mmol) of $[N(CH_3)_4][SSi(CH_3)_3]$ and a small Teflon-coated magnetic stir bar were added to a $^3/_4$-in.-o.d. FEP reactor equipped with a stainless steel valve. Subsequently, 6.219 g (86.23 mmol) of THF was vacuum-distilled onto the solid at −196 °C. The reaction mixture was then stirred at 20 °C to achieve maximum dissolution of $[N(CH_3)_4][SSi(CH_3)_3]$, which formed a clear colorless solution. Some white solid was still visible at the bottom of the reaction vessel because not all dissolved. Vacuum distillation of 0.040 g (0.13 mmol) of WF_6 at −196 °C was followed by warming of the mixture to −78 °C and stirring for ca. 1 h as the solution went from yellow to pale pink. The solvent THF was removed under dynamic vacuum overnight at −78 °C and then for 30 min at room temperature at −196 °C into a FEP U-tube, which was connected to the glass vacuum line. The reaction vessel was holding 0.060 g of a homogeneous pale-pink powder. The amount of solid recovered corresponded to 0.15 mmol of $[N(CH_3)_4][WSF_5]$, indicating the presence of a small amount of C_4H_8O in the final product. The ^1H NMR spectrum revealed a very small peak at 12.39 ppm and a broad feature at ca. 4.9 ppm, which likely correspond to an aldehyde and an aliphatic chain resulting from the ring opening of THF.

Preparation of $[N(CH_3)_4][W_2S_2F_9]$. Inside the drybox, 0.087 g (0.30 mmol) of WSF_4 and 0.013 g (0.014 mmol) of $[N(CH_3)_4][F]$ were loaded into a $^1/_4$-in.-o.d. FEP tube equipped with a Kel-F valve. Approximately 0.75 mL of CH_3CN was vacuum-distilled onto the solid. The solvent was allowed to melt at −37 °C, resulting in a deep-brown suspension. Warming to ambient temperature and agitating the reaction mixture allowed for complete reaction. The solvent was removed under dynamic vacuum, yielding 0.096 g (0.14 mmol) of brown $[N(CH_3)_4][W_2S_2F_9]$. Decomposition at 184 °C. Anal. Found: C, 6.72; H, 1.40; N, 2.42. Anal. Calcd for $C_4H_{12}F_9NS_2W_2$: C, 7.10; H, 1.79; N, 2.07.

Vibrational Spectroscopy. The Raman spectra of $[N(CH_3)_4][WSF_5]$ and $[N(CH_3)_4][W_2S_2F_9]$ were recorded on a Bruker RFS 100 Fourier transform (FT)-Raman spectrometer with a quartz beam splitter, a liquid-nitrogen-cooled germanium detector, and a low-temperature accessory. The backscattered (180°) radiation was sampled. The actual usable Stokes range was 50−3500 cm^{-1} with a spectral resolution of 2 cm^{-1}. The 1064-nm line of an Nd:YAG laser was used for excitation of the sample. The room- and low-temperature (−100 °C) Raman spectra of $[N(CH_3)_4][WSF_5]$ and $[N(CH_3)_4]$-

dx.doi.org/10.1021/ic3005882 | Inorg. Chem. 2012, 51, 6350−6359

$[W_2S_2F_9]$ were recorded on powdered samples in sealed melting point capillaries using a laser power of 200 and 150 mW, respectively. The FTIR spectrum of $[N(CH_3)_4][WSF_5]$ was recorded on a Nicolet Avatar 360 FTIR spectrometer at ambient temperature as a KBr pellet. The FTIR spectrum of $[N(CH_3)_4][W_2S_2F_9]$ was recorded at ambient temperature on a Bruker Tensor FTIR spectrometer as a KBr pellet. The KBr pellet was formed in a Wilks minipress inside the drybox by sandwiching the sample between two layers of KBr. The IR spectra were acquired in 64 scans at a resolution of 2 cm^{-1}.

NMR Spectroscopy. All NMR spectra were recorded unlocked on a 300 MHz Bruker Avance II NMR spectrometer equipped with a 5-mm broad-band probe. All NMR spectra were externally referenced to neat $CFCl_3$ (^{19}F) and neat $Si(CH_3)_4$ (^1H and ^{13}C) at 25 °C. The ^{19}F NMR spectra were typically acquired in 128K memory with spectral settings of 34 kHz, yielding an acquisition time of 1.9 s and a data-point resolution of 0.26 Hz/data point. The number of transients accumulated was between 200 and 600 using a pulse width of 10.3 μs. The ^1H /^{13}C NMR spectra were typically acquired in 64/64K memory with spectral settings of 6/18 kHz, yielding acquisition times of 5.3/1.8 s and data point resolutions of 0.09/0.27 Hz/data point. The numbers of transients accumulated were 68/9200 using pulse widths of 12.4/7.6 μs.

X-ray Crystal Structure Determination. *a. Crystal Growth. $[N(CH_3)_4][WSF_5]\cdot CH_3CN$.* A solution of about 0.100 g of $[N(CH_3)_4][WSF_5]$ in 1.0 mL of CH_3CN inside a 9-mm-o.d. FEP tube equipped with a stainless steel valve was cooled to −20 °C. About three quarters of the solvent was slowly removed under dynamic vacuum at this temperature over a period of approximately 3 h, and orange prismatic crystals were formed. Under an atmosphere of dry nitrogen, the remaining solution was decanted off, and clear orange prismatic crystals of $[N(CH_3)_4][WSF_5]\cdot CH_3CN$ were isolated. $[\mathbf{N(CH_3)_4}][\mathbf{W_2S_2F_9}]$. A solution of about 0.050 g of $[N(CH_3)_4][W_2S_2F_9]$ in 0.5 mL of anhydrous HF inside a 9-mm-o.d. FEP tube equipped with a stainless steel valve was cooled to 0 °C. The solvent was slowly removed under dynamic vacuum at this temperature over a period of 6 h, and clear yellow prismatic crystals of $[N(CH_3)_4][W_2S_2F_9]$ were obtained.

b. Crystal Mounting, Collection and Reduction of X-ray Data. Inside the drybox, several crystals were selected and dropped into a small dish containing some Krytox GPL107 oil. The dish was taken out of the drybox and the crystal trapped in a nylon cryoloop. The single-crystal diffraction data were collected on a Bruker SMART three-circle platform diffractometer,[14] equipped with an APEX charge-coupled detector with the χ-axis fixed at 54.74° and using Mo Kα radiation (λ = 0.71073 Å) from a fine-focus tube. This diffractometer was equipped with a CRYO Industries LT-3 low-temperature apparatus using controlled nitrogen boiloff. Cell constants were determined from 90 10-s frames at −155 °C ($[N(CH_3)_4][WSF_5]\cdot CH_3CN$) and −130 °C ($[N(CH_3)_4][W_2S_2F_9]$). A complete hemisphere of data was collected, using 1271 frames at 10 s $frame^{-1}$ at a detector resolution of 512 × 512 pixels, including 50 frames that were collected at the beginning and end of the data collection to determine crystal decay. The frames were processed on a PC running Windows XP using *SAINT* software.[15] Absorption correction was applied using the *SADABS* program.[16]

c. Solution and Refinement of the Structures. The structures were solved by the Patterson method, using the *SHELXS* program, and refined by the least-squares method on F^2 with *SHELXL* incorporated in *SHELXTL*, version 2011.4-0.[17] All atoms were refined anisotropically.

Crystallographic data have been deposited with the Cambridge Crystallographic Data Center as CCDC 855350 and 855351. Copies of the data can be obtained free of charge from CCDC via http://www.ccdc.cam.ac.uk.

Computational Methods. The optimized geometries and frequencies of WSF_5^- and $W_2S_2F_9^-$ were calculated at the density functional theory level by use of the B3LYP[18] method. The Stuttgart basis set augmented by one f-type polarization function (α_f = 0.823)[19] for tungsten and aug-cc-pVTZ basis sets for fluorine, nitrogen, carbon, and hydrogen was used. Pseudopotentials were used for tungsten. Quantum-chemical calculations were carried out using the programs *Gaussian 03*.[18] The geometries were fully optimized using analytical gradient methods. The vibrational frequencies were calculated at the B3LYP level using the appropriate minimized structure, and the vibrational mode descriptions were assigned with the aid of *Gaussview*.[20]

■ ASSOCIATED CONTENT

Ⓢ Supporting Information

Table with vibrational spectroscopy data of $[N(CH_3)_4][SSi(CH_3)_3]$ (Table S1), Raman and IR spectra of $[N(CH_3)_4][SSi(CH_3)_3]$ (Figure S1), thermal ellipsoid plot of the asymmetric unit of $[N(CH_3)_4][WSF_5]\cdot CH_3CN$ (Figure S2), and view of the packing of $[N(CH_3)_4][WSF_5]\cdot CH_3CN$ (Figure S3). This material is available free of charge via the Internet at http://pubs.acs.org.

■ AUTHOR INFORMATION

Corresponding Author

*E-mail: michael.gerken@uleth.ca. Tel.: +1-403-329-2173. Fax: +1-403-329-2057.

Notes

The authors declare no competing financial interest.

■ ACKNOWLEDGMENTS

M.G. thanks the Natural Sciences and Engineering Research Council of Canada and the University of Lethbridge for support of this work. R.H. is thankful for NSF CRIF Grant 1048807 supporting an X-ray diffractometer. We also thank the Fluorine Division of the American Chemical Society for a Moissan summer undergraduate research fellowship for T.R. The quantum-chemical calculations were carried out using the computational resources of the Shared Hierarchical Academic Research Computing Network (SHARCNET: www. Sharcnet.ca). We thank Kevin Johnson for carrying out elemental analyses.

■ REFERENCES

(1) Nieboer, J.; Hillary, W.; Yu, X.; Mercier, H. P. A.; Gerken, M. *Inorg. Chem.* **2009**, *48*, 11251−11258.
(2) Nieboer, J.; Yu, X.; Chaudhary, P.; Mercier, H. P. A.; Gerken, M. *Z. Anorg. Allg. Chem.* **2012**, *638*, 520−525.
(3) Buslaev, Y. A.; Kokynov, Y. B.; Chubar, Y. D. *Proc. Acad. Sci. (USSR)* **1973**, *213*, 912−914.
(4) Atherton, M. J.; Holloway, J. H. *J. Chem. Soc., Chem. Commun.* **1977**, 424−425.
(5) Hilbers, M.; Läge, M.; Mattes, R. *Inorg. Chim. Acta* **1992**, *201*, 1−3.
(6) Do, Y.; Simhon, E. D.; Holm, R. H. *Inorg. Chem.* **1983**, *22*, 3809−3812.
(7) (a) Hwu, J. R.; Tsay, S.-C. *J. Org. Chem.* **1990**, *55*, 5987−5991. (b) Hwu, J. R.; Wong, F. F.; Shiao, M.-J. *J. Org. Chem.* **1992**, *57*, 4254−5255. (c) Shiao, M.-J.; Lai, L. L.; Ku, W.- S.; Lin, P.-Y.; Hwu, J. R. *J. Org. Chem.* **1993**, *58*, 4742−4744.
(8) Christe, K. O.; Wilson, W. W.; Wilson, R. D.; Bau, R.; Feng, J.-a. *J. Am. Chem. Soc.* **1990**, *112*, 7619−7625.
(9) Kabisch, G. *J. Raman Spectrosc.* **1980**, *9*, 279−285.
(10) Goubeau, J.; Hiersmann, W. D. *Z. Anorg. Allg. Chem.* **1957**, *290*, 292−301.
(11) McFarlane, W.; Noble, A. M.; Winfield, J. M. *J. Chem. Soc. A* **1971**, 948−953.
(12) Winfield, J. M. *J. Fluorine Chem.* **1984**, *25*, 91−98.
(13) Wilson, W. W.; Christe, K. O. *Inorg. Synth* **1986**, *24*, 37−38.
(14) *SMART, Software for the CCD Detector System*, version 5.625; Bruker AXS: Madison, WI, 2001.

(15) *SAINT*, version 7.68A; Bruker AXS: Madison, WI, 2009.
(16) *SADABS*, version 2008/1; Bruker AXS: Madison, WI, 2008.
(17) *SHELXTL*, version 2011.4-0; Bruker AXS: Madison, WI, 2011.
(18) Frisch, M. J.; Trucks, G. W.; Schlegel, H. B.; Scuseria, G. E.; Robb, M. A.; Cheeseman, J. R.; Zakrzewski, V. G.: Montgomery, J. A., Jr.; Stratmann, R. E.; Burant, J. C.; Dapprich, S.; Millam, J. M.; Daniels, A. D.; Kudin, K. N.; Strain, M. C.; Farkas, O.; Tomasi, J.; Barone, V.; Cossi, M.; Cammi, R.; Mennucci, B.; Pomelli, C.; Adamo, C.; Clifford, S.; Ochterski, J.; Petersson, G. A.; Ayala, P. Y.; Cui, Q.; Morokuma, K.; Salvador, P.; Dannenberg, J. J.; Malick, D. K.; Rabuck, A. D.; Raghavachari, K.; Foresman, J. B.; Cioslowski, J.; Ortiz, J. V.; Baboul, A. G.; Stefanov, B. B.; Liu, G.; Liashenko, A.; Piskorz, P. K. I.; Gomperts, R.; Martin, R. L.; Fox, D. J.; Keith, T.; Al-Laham, M. A.; Peng, C. Y.; Nanayakkara, A.; Challacombe, M.; Gill, P. M. W.; Johnson, B.; Chen, W.; Wong, M. W.; Andres, J. L.; Gonzalez, C.; Head-Gordon, M.; Replogle, E. S.; Pople, J. A. *Gaussian 98*, revision A.11; Gaussian, Inc.: Pittsburgh, PA, 2003 (g03_D.01).
(19) Ehlers, A. W.; Bohme, M.; Dapprich, S.; Gobbi, A.; Hollwarth, A.; Jonas, V.; Kohler, K.; Segmann, F. R.; Veldkamp, A.; Frenking, G. *Chem. Phys. Lett.* **1993**, *208*, 111−114.
(20) *GaussView*, release 3.0; Gaussian Inc.: Pittsburgh, PA, 2003.

dx.doi.org/10.1021/ic3005882 | *Inorg. Chem.* 2012, 51, 6350−6359